Ultrasmall Hollow Gold–Silver Nanoshells with Extinctions Strongly Red-Shifted to the Near-Infrared

Varadee Vongsavat,[†] Brandon M. Vittur,[†] William W. Bryan,[†] Jun-Hyun Kim,[‡,*] and T. Randall Lee*,[†]

[†]Department of Chemistry, University of Houston, 4800 Calhoun Road, Houston, Texas 77204-5003, United States

[‡]Department of Chemistry, Illinois State University, Normal, Illinois 61790-4160, United States

S *Supporting Information*

ABSTRACT: Hollow gold–silver nanoshells having systematically varying sizes between 40 and 100 nm were prepared. These particles consist of a hollow spherical silver shell surrounded by a thin gold layer. By varying the volume of the gold stock solution added to suspensions of small silver-core templates, we tailored the hollow gold–silver nanoshells to possess strong tunable optical extinctions that range from the visible to the near-IR spectral regions, with extinctions routinely centered at ~950 nm. The size and morphology of these core/shell nanoparticles were characterized by dynamic light scattering (DLS), field emission scanning electron microscopy (FE-SEM), and transmission electron microscopy (TEM). Separately, X-ray diffraction (XRD), energy-dispersive X-ray spectroscopy (EDS) and X-ray photoelectron spectroscopy (XPS) were used for measuring their elemental composition; UV–vis spectroscopy was used to evaluate their optical properties. Given their relatively small size compared to other nanoparticles that absorb strongly at near IR wavelengths, these easy-to-synthesize particles should find use in applications that require ultrasmall nanoparticles with extinctions comfortably beyond visible wavelengths (e.g., medicinal therapies, diagnostic imaging, nanofluidics, and display technologies).

KEYWORDS: ultrasmall, plasmonic, nanoshells, nanoparticles, near-infrared, NIR
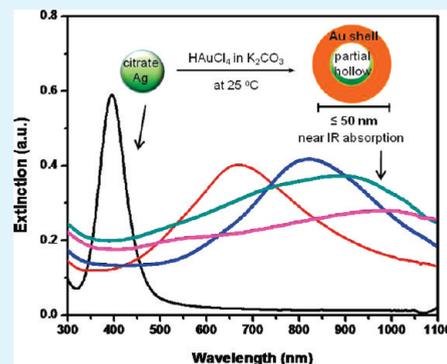
■ INTRODUCTION

Metal nanoparticles have been studied for decades because of their attractive properties and potential applications in areas such as catalysis, electronics, photonics, information storage, biosensors, and surface-enhanced Raman spectroscopy (SERS).[1−7] In particular, nanoparticles derived from noble metals, such as Au and Ag, have generated great interest due to their associated strong plasmon resonance.[8] When dispersed in liquid media, these nanoparticles display intense colors because of the surface plasmon resonance—a feature that can be attributed to the collective oscillation of conduction electrons induced by an electromagnetic field.[9] The surface plasmon resonance of nano-sized metal particles is different from that of bulk materials and depends strongly on the size, shape, and degree of aggregation of the nanoparticles, as well as the dielectric properties of the surrounding medium.[9,10]

Metal nanoshells are unique composite nanoparticles that consist of a spherical dielectric nanoparticle core[11] covered by a thin metallic shell.[12−15] These types of nanoshells possess optically responsive properties favorable for use in biomedical imaging and therapeutic applications.[1,16] In particular, metal nanoshells exhibit strong plasmon resonances that are typically shifted to much longer wavelengths than the plasmon resonance of corresponding solid metal nanospheres.[13,15] By varying the relative dimensions of the shell/core layers, the optical resonance of these nanoparticles can be precisely and systematically varied over a broad range of wavelengths that span the UV–vis and near–IR spectral regions.[13,17] The near–IR region is particularly relevant for biomedical applications because light at wavelengths between 800 and 1200 nm can penetrate both water and human tissue.[18] This range of wavelengths is referred to as the "tissue-transparency window".[19] Exploiting this window by using optically active nanoparticles gives rise to applications as photo-thermal energy converters in a range of applications that includes photothermal cancer therapy[1,20] and photothermally triggered drug release.[15,21−23] For these therapies, it is important to position the absorption of the nanoparticles well beyond the visible range to allow optical modulation completely outside the realm of any known organic chromophores. This strategy will minimize damage to healthy tissue.

In contrast to the attractive optical properties of conventional nanoshells, certain features stand as major roadblocks to their widespread use in everyday applications. Most notably, the synthetic preparation of nanoshells is tedious and time-consuming. Furthermore, it is difficult to prepare duplicate batches of nano-shells exhibiting the same structural dimensions and/or optical properties. A second important drawback centers on the fact that it is extremely difficult to prepare nanoshells with dimensions smaller than 100 nm. Consequently, applications that require

Bimetallic Nanoparticles   Bimetallic Hollow Nanoshells
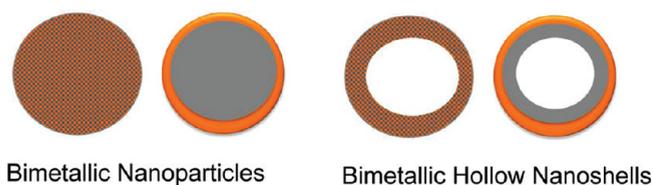
Figure 1. Illustrations of bimetallic nanoparticles and bimetallic hollow gold—silver nanoshells, where alloy structures are shown on the left and layered structures on the right.

components smaller than 100 nm cannot utilize conventionally prepared nanoshells. To this end, there were two recent reports of nanoshells with dimensions smaller than conventional nanoshells: gold-coated gold sulfide nanoshells (i.e., Au/Au_2S, with diameters 35-55 nm)[24] and gold-silica-gold nanoshells ($Au/SiO_2/Au$, with diameters 85—170 nm).[25] The smaller Au/Au_2S particles offer additional benefits for tumor ablation in cancer therapy through improved access to tumors and uptake into cells; these particles are also relatively easy to manufacture.[24] Similarly, our research focuses on the development of new types of nanoshell systems, such as the bimetallic or metal/metal "hollow nanoshells" described in this report.

Many groups have reported the synthesis of metal/metal nanoshells. For example, Morriss and Collins synthesized Ag/Au shell/core nanoparticles via the reduction of slightly alkaline $HAuCl_4$ solution with phosphorus and successive reduction of Ag_2O with $NH_2OH \cdot HCl$.[26] Separately, Yang and co-workers prepared Au/Ag shell/core nanoparticles via the replacement reaction between hydrophobized Ag nanoparticles and hydrophobized $[AuCl_4]^-$ in toluene.[27] Furthermore, Hu and co-workers reported the synthesis of Pd/Au shell/core nanoparticles with controllable sizes by using the chemical deposition of Pd over Au seeds.[28] Separate studies by Chen and co-workers described the synthesis of Pt/Ag shell/core nanoparticles via a seeded-growth method, which involved the treatment of Ag core particles with K_2PtCl_2 and trisodium citrate as the reducing agent.[29] The optical extinction of these metal/metal nanoshells is tunable, but still limited to visible wavelengths. In an effort to extend the optical extinction to substantially longer wavelengths, we introduce here a new route to bimetallic Au/Ag shell/core nanoparticles that possess a partially hollow core structure.

A hollow metal/metal nanoshell is a bimetallic nanoparticle that encircles a hollow or partially hollow interior (see Figure 1). We are interested in hollow metal/metal nanoshells because of their potential as plasmonic materials with extinction wavelengths markedly longer than the bimetallic nanostructures described in the preceding paragraph (i.e., with ready access to near-IR wavelengths). Importantly, methods for preparing related Au—Ag nanocages based on galvanic replacement in aqueous solution have been reported. However, the ready availability of ultrasmall nanoparticles (e.g., <50 nm in diameter) and near-IR extinctions beyond the UV—vis (i.e., >900 nm wavelengths) remains largely elusive, as does a detailed description of the mechanism(s) giving rise to the structure, composition, and morphology of these highly attractive and unique nanostuctures.

Several methods for the synthesis of Au—Ag nanostructures have been proposed, including metal-vapor techniques,[18] electrochemical pathways,[37] thermal decomposition,[38] and photochemical routes.[39,40] The most common and powerful method involves wet chemical preparations that rely on the chemical reduction of metal salts in the presence of specific surfactants at high reaction temperature (i.e., ≥ 100 °C).[31,36,41] With regard to plasmonic nanoparticles smaller than 100 nm in diameter, Jiang and co-workers reported a reliable approach for the preparation of hollow gold nanospheres with ∼60 nm diameters using small Co nanoparticles as sacrificial templates;[42] these hollow particles exhibited extinction maxima at ≤650 nm regardless of the size of the hollow cores and the thickness of the gold shells. The synthesis was further developed by Zhang and co-workers to generate hollow gold nanoshells with tunable extinctions ranging from 500 to 820 nm.[43,44] Furthermore, Xia's group prepared spherical 14 nm Au—Ag nanoparticles with extinction maxima at 740 nm,[45] spherical 23.5 nm Au—Ag nanoparticles with extinction maxima at 791 nm,[46] and Au—Ag nanocages having average body-centered diagonal lengths of ∼65—85 nm with extinction maxima ranging from 600-1200 nm.[47−50] Although the plasmon resonances of these nanoparticles were successfully tuned across much of the visible spectrum and into the near infrared, the extinction maxima of those particles smaller than ∼60 nm in diameter appear at markedly shorter wavelengths than those prepared using our strategy (vide infra).

In this work, we demonstrate the synthesis of spherical silver nanoparticle templates prepared by the reduction of silver salts using the mild reducing agent, sodium citrate. Subsequently, these spherical nanoparticles are used as templates from which to grow ultrasmall hollow gold—silver nanoshells at room temperature using a potassium-containing basic solution of gold salt, which we refer to as K-gold solution (vide infra). By varying the volume of the gold stock solution added to suspensions of small silver-core templates with sizes ranging from 40—100 nm without introducing any surfactant, these metal/metal hollow nanoshells can be tailored to possess strong tunable optical extinctions that range from the visible to the near-IR spectral regions, with extinction maxima readily tunable to greater than 900 nm. Although this method appears quite similar to those reported recently,[46,51] the hollow Au—Ag nanoshells generated by the prior methods exhibit extinction maxima at wavelengths no longer than ∼790 nm for particles smaller than ∼60 nm in diameter; in contrast, our method affords nanoshells with extinction maxima at 950—1000 nm for particles as small as 40 nm in diameter.

■ EXPERIMENTAL SECTION

Materials. Silver nitrate (Mallinckrodt), trisodium citrate dehydrated (Aldrich), potassium carbonate (J. T. Baker), hydrogen tetrachloroaurate(III) hydrate (Strem), nitric acid (EM Science), hydrochloric acid (EM Science) were purchased from the indicated suppliers and used without purification. Water was purified to a resistance of 18 MΩ (Academic Milli-Q Water System; Millipore Corporation) and filtered through a 0.22 μm membrane filter before use. All glassware was cleaned in an aqua regia solution ($HCl:HNO_3$; 3:1), thoroughly rinsed with Milli-Q water, and then dried prior to use.

Preparation of Silver Nanoparticle Cores. Silver nanoparticles of varying size were prepared by the method of Lee and Miesel,[52] which involves the reduction of $AgNO_3$ by sodium citrate. An aliquot of $AgNO_3$ (0.0334 g, 0.20 mmol) was dissolved in 200 mL of H_2O. The solution was brought to reflux, and then 2 mL of 1% trisodium citrate solution was added under vigorous stirring. The solution was allowed to reflux for 45 min. A faint yellow color was observed in the solution, indicating the formation of silver nanoparticles. The colloidal dispersion

was allowed to cool and then filtered through a 0.22 μm membrane filter. This procedure affords monodisperse silver nanoparticles having diameters that can be adjusted from 40 to 100 nm, where the size depends on the relative concentrations of the reactants.

Preparation of Hollow Gold—Silver Nanoshells. As described previously,[15,53] a potassium-containing basic solution of gold salt (K-gold solution) was prepared by adding 0.025 g of potassium carbonate (K_2CO_3) to 100 mL of Milli-Q water, and then 2 mL of 1% $HAuCl_4 \cdot H_2O$ solution was added under vigorous stirring. The mixture changed from a yellow color to colorless after the reaction had proceeded for an additional 30 min. Finally, the flask was covered with aluminum foil to shield it from light, and the solution was preserved in the refrigerator for 12 h before being used.

Gold was deposited by treatment of the silver nanoparticles with K-gold solution. In a typical procedure, 2 mL aliquots of silver colloid were placed in small vials under vigorous stirring. Varying amounts of K-Gold solution (0.2—6 mL) were added to separate vials to produce nanoparticles with varying gold content. Each mixture was stirred for at least 10 min, and the color was observed to change from light yellow to purple, dark blue, or blue depending on the core-shell dimensions. The mixture was left at room temperature for at least one day to achieve complete coating and later centrifuged at 2500 rpm for 30 min using an RC-3B refrigerated centrifuge (Sorvall Instruments), and redispersed in Milli-Q water prior to analysis.

Characterization Methods. The size and morphology of the composite nanoparticles were characterized by field emission scanning electron microscopy (FE-SEM), transmission electron microscopy (TEM), and dynamic light scattering (DLS). For the FE-SEM measurements, a JEOL JSM 6330F instrument was used, operating at an accelerating voltage of 15 kV. For the TEM measurements, a JEOL JEM-2000 FX electron microscope was used, operating at an accelerating voltage 200 kV. The samples were prepared by placing small aqueous drops of the dispersed metal nanoshells on a silicon wafer (for FE-SEM) or a copper grid (for TEM) and allowing the solvent to evaporate. The DLS data were collected using an ALV-5000 Multiple Tau Digital Correlation instrument operating with a 514.5 nm light source at a fixed scattering angle of 90°. The sample diameters measured by DLS were consistent with the values obtained by FE-SEM and TEM. The FE-SEM images were processed using the Java-based "ImageJ" program, and the size histograms were constructed from the analysis of at least 200-300 particles. X-ray diffraction was performed using a D-5000 with monochromatic Cu Kα radiation (λ = 1.540562 Å) to confirm the structure. Energy-dispersive X-ray spectroscopy (EDX) analysis measurements were collected using oxford EDX attached to the TEM microscope. The data were analyzed using INCA software, Oxford Instruments) to afford the elemental composition of the nanoparticles. Similarly, X-ray photoelectron spectrometry (XPS) measurements were analyzed using a PHI 5700 XPS equipped with monochromatic Al Kα X-ray source. All UV visible spectra were recorded at room temperature on a Cary 50 Scan UV—visible spectrometer over the wavelength range of 250—1100 nm.

■ RESULTS AND DISCUSSION

Colloidal silver particles having various sizes were prepared by reducing selected aliquots of an aqueous $AgNO_3$ solution with sodium citrate. From the SEM images and DLS measurements, silver nanoparticles with diameters of 40 $\pm$ 5, 60 $\pm$ 5, 80 $\pm$ 7, and 100 $\pm$ 9 nm were prepared by judiciously choosing the relative amounts of the reactants and by controlling the heating rate. Notably, increased heating rates led to smaller particles. The detailed reaction conditions employed in the particle synthesis are summarized in Table 1. SEM images of

Table 1. Conditions for the Preparation of Silver Nanoparticles Having Different Diameters

particle size (nm)	reactant (mmol)	reducing agent (mL)	size standard deviation (nm)
100	0.3	2	9
80	0.2	2	6
60	0.1	2	4
40	0.1	5	5

these silver nanoparticle cores and their corresponding particle size distribution are provided in Figure 2.

Morphology of the Hollow Gold—Silver Nanoshells. The growth of the hollow gold—silver nanoshells was achieved using an established replacement reaction.[34] By varying the amounts of K-gold solution added to an aqueous stock solution of silver nanoparticles, a series of unique bimetallic nanoparticles with hollow cores was produced. As detailed in the following paragraphs, Figures 3 and 4 and Figures S1—S3 in the Supporting Information show SEM and TEM images of 100, 80, 60, and 40 silver nanoparticles before and after they were treated with selected volumes of K-gold solution (individually, not successively). Upon the addition of a small aliquot of K-gold solution, a small pinhole (or pinholes) form(s) at the surface of the particles due to the oxidation of Ag by Au.[45] When larger aliquots of K-gold solution are added to the silver core particles, the pinholes grow into larger cavities. At a critical volume of added K-gold solution, which varies depending on the size of the core particle, a gold shell encapsulates the particle, leading to a bimetallic having a partial hollow interior (see Figure 1). We believe that this mechanism is operative for all of the particles studied in this investigation.

Figure 3 shows SEM images of the 100 nm silver core particles before and after treatment with K-gold solution. In these samples, the cavities become clearly discernable only after the addition of $\geq$1 mL of the solution (i.e., Figure 3c,d). For the 80 nm silver core particles, the point at which the cavities become discernable is more difficult to judge by SEM (see Figure S1 in the Supporting Information); however, imaging of these particles by TEM reveals the appearance of pinholes and the growth of cavities immediately upon the addition of the K-gold solution (see Figure 4). In these images, the deposition of gold atoms on the silver core to form bimetallic nanoparticles and the formation of hollow cores can be discerned by noting the difference in contrast between inner and outer regions of the particles.[54] In Figure 4, pinholes become visible upon the addition of 0.8 mL of K-gold solution (Figure 4b), and larger holes can be discerned with the addition of larger volumes of K-gold solution (Figure 4c,d). Increasing the amount of K-gold solution added past 1 mL up to a critical volume of 3 mL leads to the deposition of a gold shell on the exterior of the particle with a concomitant etching of the Ag core to create a hollow interior.[31] At 3 mL of K-gold solution added, a complete or nearly complete Au shell is formed (Figure 4e). In contrast, the critical volume required for partial core removal and complete shell formation for the 60 nm core particles is 5 mL (see Figure S2 in the Supporting Information), whereas that for the 40 nm core particles is 1.5 mL (see Figure S3 in the Supporting Information). Please note that the critical volumes listed here for each nanoparticle core size were determined by visual inspection of the color of the nanoparticle solutions and the corresponding
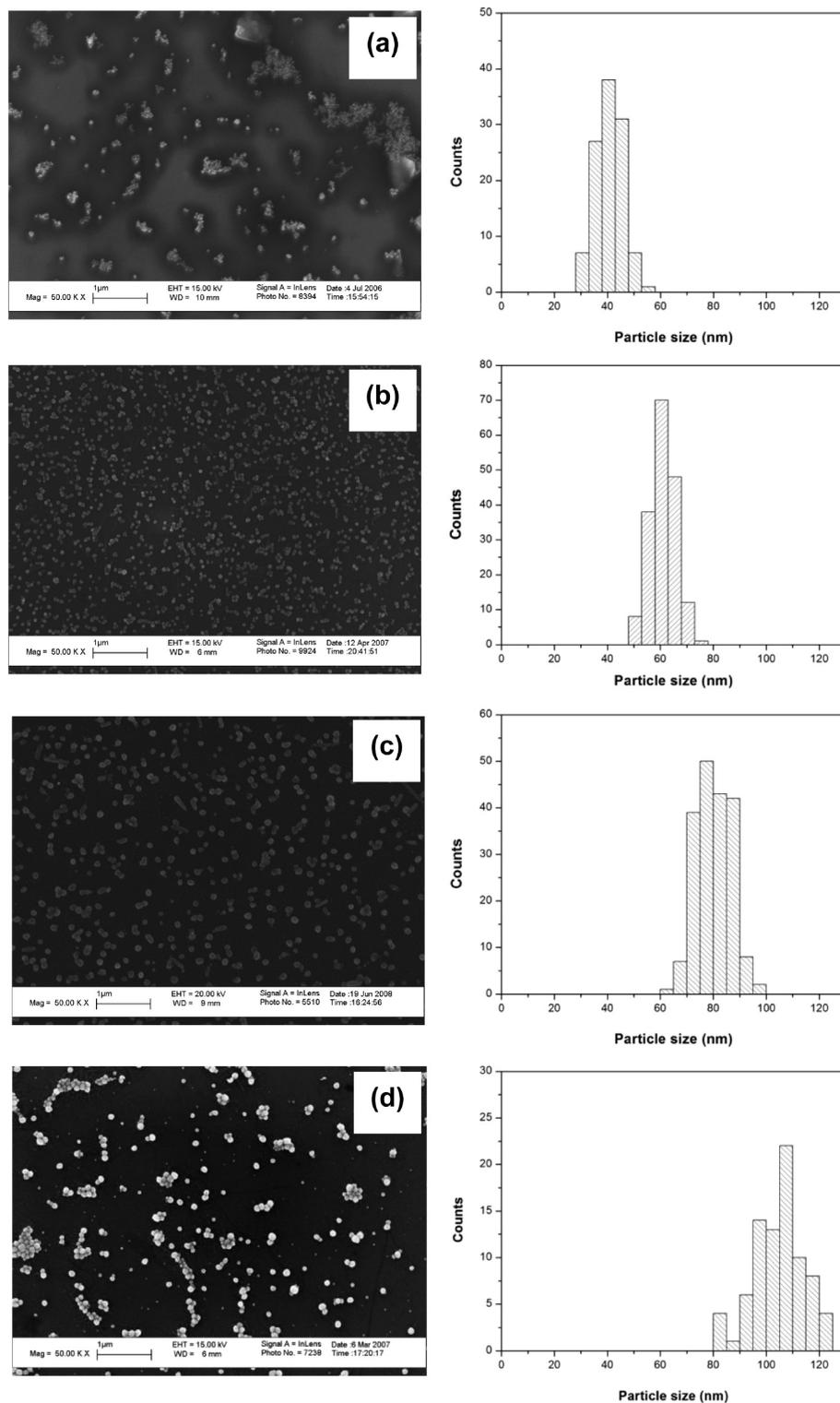
Figure 2. SEM images of silver nanoparticle cores and particle size distributions: (a) ∼40, (b) ∼60, (c) ∼80, and (d) ∼100 nm in diameter.

SEM and TEM images of the particles in the differently colored solutions. Also, the variance in the volume amounts is probably due to concentration differences between the various batches of nanoparticles.

Composition of the Hollow Gold—Silver Nanoshells. We used XRD, EDX, and XPS to characterize the elemental composition of

the hollow gold—silver nanoshells formed by the replacement reaction. Figure 5 shows the XRD patterns of pure Ag, Au, and bimetallic Au/Ag nanoparticles. For pure Au nanoparticles (Figure 5a), a strong band is observed at $2\theta = 38.14$ and 45.39, which corresponds to the (111) and (200) crystallographic planes. Three additional peaks appear at $2\theta = 64.54$, 77.50, and 81.67, which

3619

dx.doi.org/10.1021/am2008322 |*ACS Appl. Mater. Interfaces* 2011, 3, 3616–3624
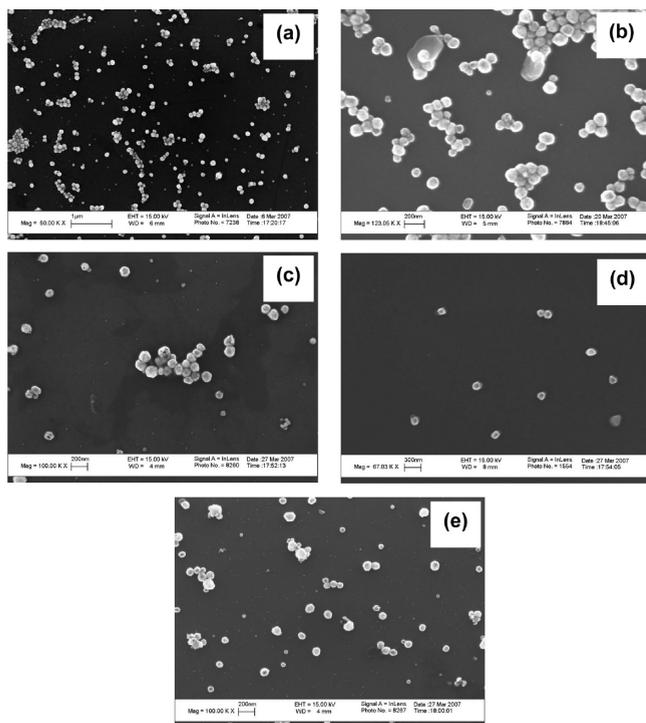
Figure 3. SEM images of (a) silver nanoparticles ∼100 nm in diameter after reaction with (b) 0.5, (c) 1, (d) 2, and (e) 4 mL of K-gold solution.
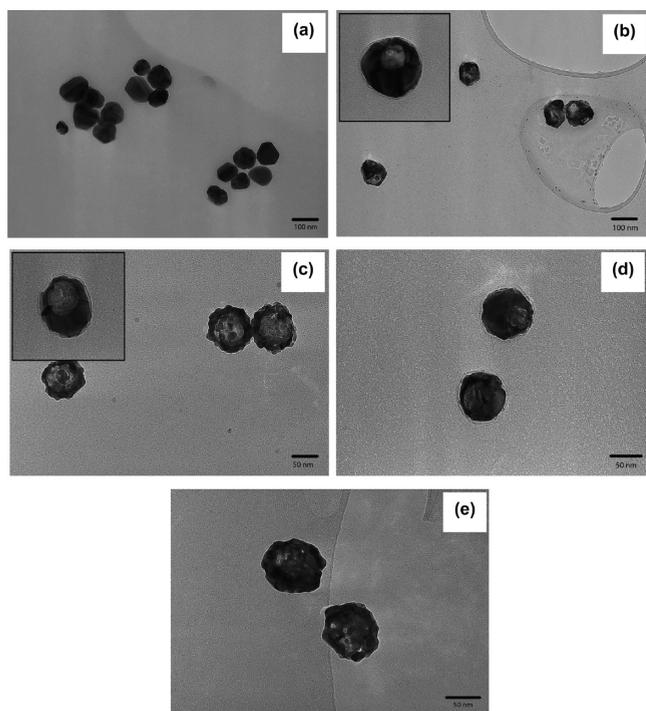
Figure 4. TEM images of (a) silver nanoparticles ∼80 nm in diameter after reaction with (b) 0.8, (c) 1.0, (d) 1.5, and (e) 3.0 mL of K-gold solution.

correspond to the (220), (311), and (222) crystallographic planes, respectively. For pure Ag nanoparticles (Figure 5b), a strong band is observed at $2\theta = 38.05$ and 45.20, which corresponds to the (111)
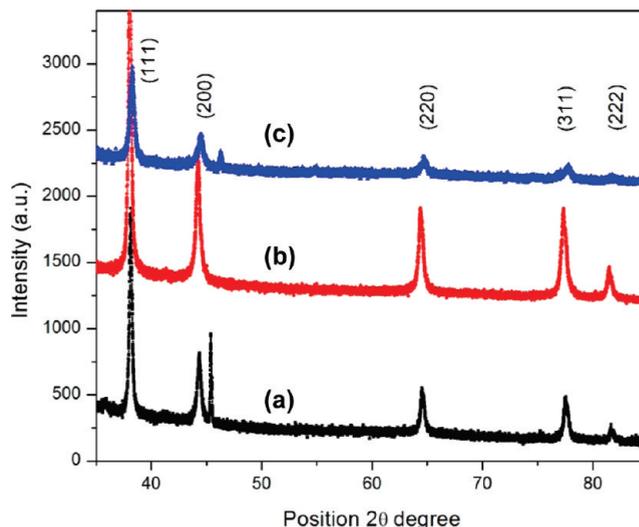
Figure 5. XRD spectra of (a) gold nanoparticles, (b) silver nanoparticles (∼80 nm), and (c) the ∼80 nm silver nanoparticles after 1.5 mL of K-gold solution was added.

Table 2. EDX-Determined Elemental Ratios of 80 nm Hollow Au−Ag Nanoshells as a Function of the Amount of K-Gold Solution Added

K-gold solution (mL)	Ag	Au	Ag/Au
0.8	52.96	4.26	12.43
1.0	38.05	5.49	6.93
1.5	32.58	9.36	3.48
3.0	11.87	3.61	3.29

and (200) crystallographic planes. The three additional peaks at $2\theta = 64.38$, 77.36, and 81.77 corresponding to the (220), (311), and (222) crystallographic planes, respectively. In the case of the Au/Ag bimetallic nanoparticles (Figure 5c), the peaks appear at $2\theta = 38.27$, 45.02, 64.76, and 77.80, which correspond to the (111), (200), (220), and (311) crystallographic planes, respectively. These results show that all reflections are similar, with similar lattice constants, d-values, and 2θ values that lie extremely close to each other (JCPDS 4-083, 4-0784).[55] We note also that a peak at $2\theta = 45.5$ appears in the XRD patterns of the pure Au nanoparticles and the Au/Ag bimetallic nanoparticles (Figures 5a and 5c); this peak is characteristic of NaCl, which can plausibly be produced from the reaction between $HAuCl_4$ and trisodium citrate.

Figure S4 in the Supporting Information shows the EDX spectrum of the ∼80 nm silver nanoparticles after 1.0 mL of K-gold solution was added. The spectrum confirms the presence of gold peaks (Mα and Lα) at 2.12 and 9.71 keV, respectively, and characteristic peaks of silver (Lα and Lβ) at 3.05 and 3.20 keV, respectively. Also a small peak characteristic of copper is observed from the supporting copper grid used for analysis. We also used EDX to determine the elemental ratio of gold and silver in the nanostructures. Table 2 shows the Ag/Au ratio determined by EDX for the ∼80 nm silver nanoparticles after adding selected volumes of K-gold solution. The asymptotically decreasing trend in these data is consistent with a growth model in which Au was deposited on the surface, and Ag was partially dissolved from the interior, giving rise to the formation of a hollow structure. Similar

Table 3. XPS-Determined Elemental Ratios of 80 nm Hollow Au−Ag Nanoshells as a Function of the Amount of K-Gold Solution Added

K-gold solution (mL)	intensity			atomic concentration		
	Ag	Au	Ag/Au	Ag	Au	Ag/Au
0.8	6262.18	1031.94	6.06	20.84	3.17	6.57
1.0	12112.96	2804.41	4.32	35.16	7.51	4.68
1.5	7634.05	5233.11	1.46	25.84	16.34	1.58
3.0	12139.17	8530.50	1.42	27.18	17.62	1.54

trends were observed for all of the silver nanoparticle cores. Furthermore, the ratio of Ag/Au reached a plateau of ~3.0 for all of the nanoparticle sizes examined.

We also employed XPS to measure the ratio of silver to gold in the nanostructures. Figure S5 in the Supporting Information shows the XPS spectrum of the 80 nm silver core particles after the addition of 1.0 mL of K-gold solution. Figure S5a in the Supporting Information shows the Ag(3d) peaks observed at binding energies of 368.1 and 374.2 eV, whereas Figure S5b in the Supporting Information shows the Au(4f) peaks at 83.9 and 87.7 eV. On the basis of a standard deconvolution of the peak intensities, the elemental ratios of Ag to Au in the nanostructures as a function of K-gold solution added are summarized in Table 3. The XPS data are consistent with the EDX data in the sense that both analyses confirm an asymptotic decrease in the Ag/Au ratio for the bimetallic nanoparticles as the amount of K-gold solution was increased. As a whole, these data are consistent with the SEM and TEM images, which are collectively consistent with a model in which Ag is partially lost from the inside of each particle to afford a hollow interior while a complete gold shell forms on the exterior. We are confident that the shell is complete because both the EDX and the XPS data ultimately plateau and remain constant, with no further changes in the ratio of Ag/Au (i.e., both Au shell formation and Ag interior etching cease once the shell growth is complete, and the pinholes have been sealed).

Importantly, a side-by-side comparison of the EDX and XPS data provides strong evidence for the formation of partially hollow gold−silver nanoshells in which gold is concentrated on the outermost region of the bimetallic shell. When characterizing metal nanoparticles ~80 nm in diameter, EDX samples the bulk composition of the particles, while XPS is a surface-sensitive technique, sampling only the outermost region of the particles. Specifically, the Ag/Au ratio of the hollow gold−silver nanoshells measured by EDX is higher than that measured by XPS because the electron beam in EDX can probe to a depth of 1-2 micrometers, while XPS can probe to a depth of no more than 10 nm.[56,57] A previous study by Liz-Marzán and co-workers using the scanning transmission electron microscopy-X-ray energy dispersive spectroscopy (STEM-XEDS) provides independent support for the proposed structural model.[58] Specifically, their elemental mapping of galvanically generated multishell bimetallic Au@Ag@Au nanoparticles showed that Au is located largely in the outer shell, and Ag is located beneath the shell, leaving a small void space at the core of the particle. Although the analyses by STEM-XEDS, XRD, EDX, and XPS analyses do not rule out the possibility of alloy formation, the data strongly suggest the separation of gold and silver in the particles; moreover, the observed long extinction wavelengths (vide infra) are consistent with gold shells rather than alloy or silver shells.[15]

Scheme 1. Proposed Reaction between Silver Nanoparticles and K-Gold Solution
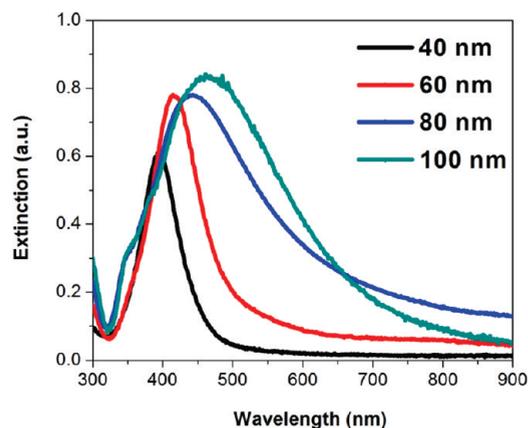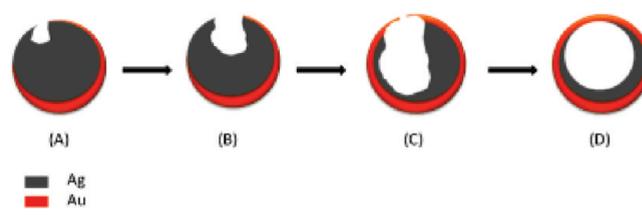
Figure 6. UV−vis spectra of silver nanoarticles having four distinctive sizes.

Scheme 1 provides an illustration of the proposed galvanic replacement reaction between the Ag(0) nanoparticle cores and the Au(III) K-gold solution.[30−36,50,58] Upon the addition of K-gold solution, the Au atoms begin to deposit on the Ag nanoparticle surface, which leads to the formation of an incomplete Au shell. At the same time, the Ag(0) core begins to oxidize and generates a pinhole on the surface. As the K-gold solution continuous to deposit Au(0) on the surface, a larger cavity is generated in the interior with concomitant formation of Ag(I). As the Au(0) continues to deposit onto the exterior of the Ag nanoparticle, the Au shell becomes complete, and a bimetallic gold−silver nanoshell with a partial hollow cavity is produced.

Optical Properties of the Gold-Coated Silver Nanoparticles. Figure 6 shows the extinction spectra of silver nanoparticles having four distinct sizes. The plasmon resonance is strong, and its maximum red-shifts with increasing particle diameter ($\lambda_{max} = $ 392, 419, 438, and 461 nm for the 40, 60, 80, and 100 nm particles, respectively). Notably, our purification method, which involves membrane filtration to eliminate any aggregated Ag nanoparticles before the addition of K-gold solution, can plausibly lead to a variation in the concentration of Ag nanoparticles across the various size-specific stock solutions. Consequently, it is difficult to compare the red shifts for a given volume of added K-gold across the different sizes of Ag nanoparticles. However, for a given size of Ag nanoparticle, the concentrations are the same for each volume of K-gold added, which allows for ready monitoring of the shift of the surface plasmon resonance in these cases.

This result indicates that the plasmon resonance depends explicitly on the particle size, which can be rationalized by Mie theory.[59] When small volumes of K-gold solution were added to
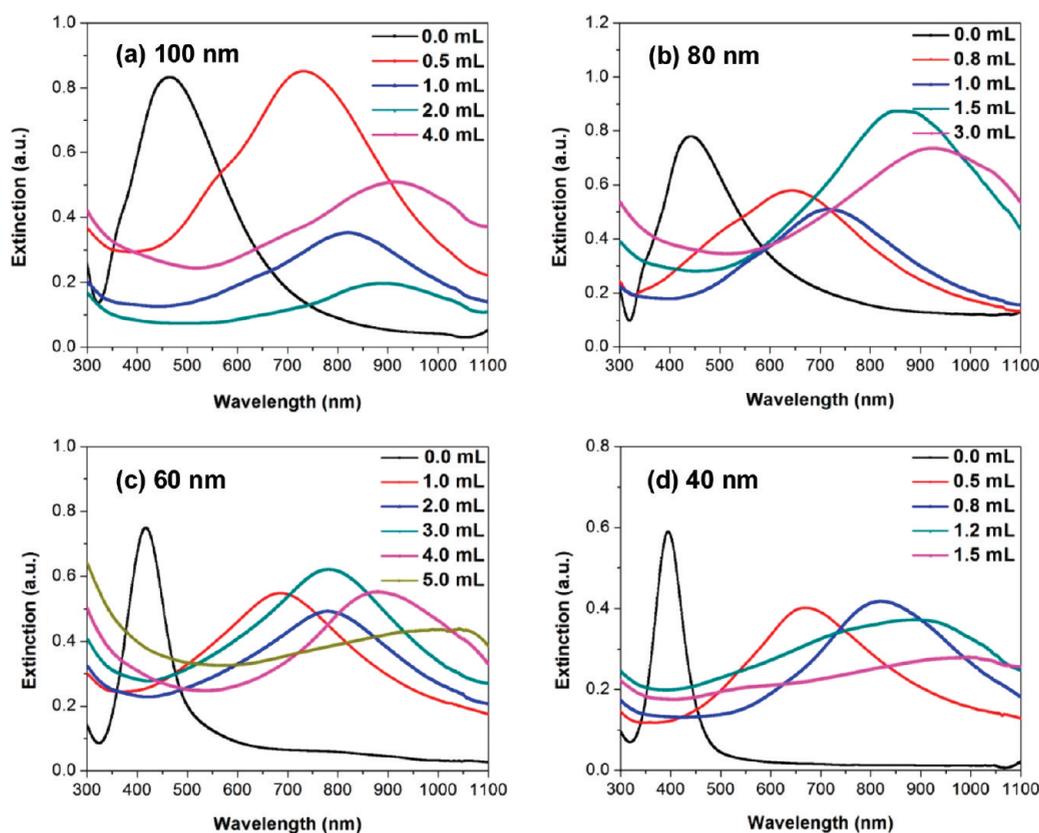
Figure 7. UV−vis spectra of (a) 100, (b) 80, (c) 60, and (d) 40 nm particles before and after reaction with different volumes of K-gold solution.
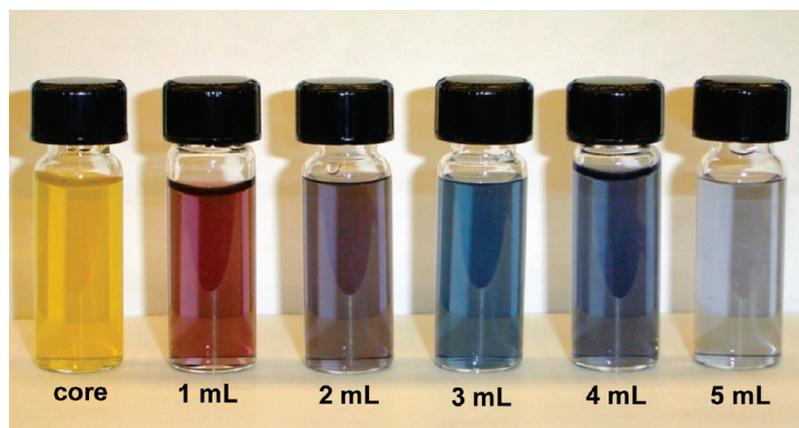
Figure 8. Photographs of aqueous dispersions of ∼60 nm silver nanoparticles before and after reaction with selected aliquots of K-gold solution.

the aqueous dispersions of silver nanoparticles, the extinction maxima were red-shifted to relatively long wavelengths. Figure 7 shows the extinction spectra of 100 nm, 80 nm, 60 nm, and 40 nm particles before and after reaction with different volumes of K-gold solution. The 100 nm core particles have an initial extinction maximum at 461 nm. The volumes of K-gold solutions were subsequently doubled beginning at 0.5 mL up to 4 mL. At 0.5 mL, the extinction maximum is red-shifted to 735 nm. At 1 mL, an extinction maximum of 820 nm is achieved. At 2 mL, an extinction maximum of 875 nm is observed. A red shift to 925 nm was achieved upon addition of 4 mL of K-gold solution. For the 80 nm particles, the initial extinction maximum appears at

438 nm and red-shifts to a maximum at 937 nm upon the addition of 3 mL of K-gold solution. The 60 nm particles exhibit an initial extinction maximum at 419 nm and reach a maximum at 1050 nm upon the addition of 5 mL of K-gold solution. The 40 nm particles exhibit an initial extinction maximum of 392 nm, which red-shift to 1000 nm after the addition of 1.5 mL of K-gold solution.

These spectral changes can be attributed to the deposition of thin gold layers on the surface of the silver nanoparticle templates.[58] The broadness and intensity of the surface plasmon band depends primarily on the shape and coverage of the gold shell.[60,61] As the volume of added K-gold solution is increased,

the extinction bands broaden and systematically shift to longer wavelengths -- eventually into the near-IR region. These red-shifts in band position are believed to be related to the formation of pinholes in the composite nanoparticles.[62,63] Importantly, the use of K-gold in this galvanic replacement reaction appears to be responsible for the extreme red-shifts observed in the extinction spectra of our nanoparticles when compared to those of similar hollow gold and gold—silver nanoshells (vide supra). Although we do not presently understand the mechanism(s) giving rise to this difference, we note that solution pH has been shown to play an important role in tuning the morphology and optical properties of gold colloids synthesized by wet chemical methods, with higher pH values leading to particles with longer extinction wavelengths.[64,65] We wish to address this issue more definitively in future studies.

Figure 8 shows a photograph of six aqueous solutions of ~60 nm gold-coated silver nanoparticles, demonstrating that the color can be tuned from yellow to blue to colorless, with the latter particles absorbing in the near IR rather than the visible. The tuning of the optical properties was accomplished by the structural transformation from solid silver nanoparticles to Au—Ag hollow gold—silver nanoshells of varying composition. This demonstration of optical tuning highlights the potential use of these metal nanostructures in applications that require ultra-small nanostructures with high extinction coefficients in the near-IR region.[48,63,66−68]

CONCLUSIONS

This report demonstrates the growth of partially hollow gold—silver nanoshells. Monodispersed silver core particles ranging systematically from 40 to 100 nm were obtained by the reduction of silver nitrate with sodium citrate. Treatment of these particles with K-gold solution led to rapid etching of the silver core and concomitant deposition of gold on the surface of the particles. The morphology, composition, and optical properties of the resultant metal/metal hollow nanoshells were characterized by FE-SEM, TEM, EDX, XRD, XPS, and UV-vis spectroscopy. By varying the volume of the K-gold solution added to the suspension of Ag templates, the plasmon resonance of the hollow gold—silver nanoshells were generally broad tunable to specific wavelengths across the visible and near-infrared regions of the electromagnetic spectrum. These new nanostructures are attractive for use in applications that require small nanoparticles with strong extinctions in these spectral regions.

ASSOCIATED CONTENT

ⓢ Supporting Information. SEM images showing the growth of the 80 nm nanoshells; TEM images showing the growth of the 60 nm and 40 nm nanoshells; EDX and XPS spectra of the 80 nm nanoshells (PDF). This material is available free of charge via the Internet at http://pubs.acs.org.

AUTHOR INFORMATION

Corresponding Author
*E-mail: jkim5@ilstu.edu (J.-H.K.); trlee@uh.edu (T.R.L.).

ACKNOWLEDGMENT

REFERENCES

(1) Loo, C.; Lowery, A.; Halas, N.; West, J.; Drezek, R. *Nano Lett.* **2005**, *5*, 709.

(2) Murphy, C. J.; Jana, N. R. *Adv. Mater.* **2002**, *14*, 80.

(3) Nicewarner-Pena, S. R.; Griffith Freeman, R.; Reiss, B. D.; He, L.; Pena, D. J.; Walton, I. D.; Cromer, R.; Keating, C. D.; Natan, M. J. *Science* **2001**, *294*, 137.

(4) Zhou, Q.; Zhao, H.; Pang, F.; Jing, Q.; Wu, Y.; Zheng, J. *J. Phys. Chem. B* **2007**, *111*, 514.

(5) Kim, S.-W.; Kim, M.; Lee, W. Y.; Hyeon, T. *J. Am. Chem. Soc.* **2002**, *124*, 7642.

(6) Tessier, P. M.; Velev, O. D.; Kalambur, A. T.; Rabolt, J. F.; Lenhoff, A. M.; Kaler, E. W. *J. Am. Chem. Soc.* **2000**, *122*, 9554.

(7) Sajanlal, P. R.; Pradeep, T. *Langmuir* **2010**, *26*, 8901.

(8) Liz-Marzan, L. M. K., P., V., *Nanoscale Materials*; Kluwer Academic Publishers: Dordrecht, The Netherlands, 2003.

(9) Bohren, C. F.; Huffman, D. R., *Absorption and Scattering of Light by Small Particles*; Wiley: New York, 1983.

(10) Klabunde, K. J., *Nanoscale Materials in Chemistry*; Wiley-Interscience: New York, 2001.

(11) Stober, W.; Fink, A.; Bohn, E. *J. Colloid Interface Sci.* **1968**, *26*, 62.

(12) Zhou, H. S.; Honma, I.; Komiyama, H. *Phy. Rev B* **1994**, *50*, 12052.

(13) Oldenburg, S. J.; Averitt, R. D.; Westcott, S. L.; Halas, N. J. *Chem. Phys. Lett.* **1998**, *288*, 243.

(14) Pham, T.; Jackson, J. B.; Halas, N. J.; Lee, T. R. *Langmuir* **2002**, *18*, 4915–4920.

(15) Kim, J.-H.; Bryan, W. B.; Lee, T. R. *Langmuir* **2008**, *24*, 11147.

(16) Day, E. S.; Thompson, P. A.; Zhang, L.; Lewinski, N. A.; Ahmed, N.; Drezek, R. A.; Blaney, S. M.; West, J. L. *J. Neurooncol.* **2011**, *104*, 55.

(17) Oldenburg, S. J.; Jackson, J. B.; Westcott, S. L.; Halas, N. J. *Appl. Phys. Lett.* **1999**, *75*, 2897.

(18) Kumar, C. S. S. R.; Hormes, J.; Leuschner, C., *Nanofabrication Towards Biomedical Applications*; Wiley: New York, 2005.

(19) Simpson, C. R. K., M.; Essenpreis, M.; Cope, M. *Phys. Med. Biol.* **1998**, *43*, 2465.

(20) Lowery, A. R.; Gobin, A. M.; Day, E. S.; Halas, N. J.; West, J. L. *Int. J. Nanomed.* **2006**, *1*, 1.

(21) Gorelikov, I.; Field, L. M.; Kumacheva, E. *J. Am. Chem. Soc.* **2004**, *126*, 15938.

(22) Das, M.; Sanson, N.; Fava, D.; Kumacheva, E. *Langmuir* **2007**, *23*, 196.

(23) Sershen, S. R.; Westcott, S. L.; Halas, N. J.; West, J. L. *J. Biomed. Mater Res.* **2000**, *51*, 293.

(24) Gobin, A. M.; Watkins, E. M.; Quevedo, E.; Colvin, V. L.; West, J. L. *Small* **2010**, *6*, 745.

(25) Bardhan, R.; Mukherjee, S.; Mirin, N. A.; Levit, S. D.; Nordlander, P.; Halas, N. J. *J. Phys. Chem. C* **2010**, *114*, 7378.

(26) Morriss, R. H.; Collins, L. F. *J. Chem. Phys.* **1964**, *41*, 3357.

(27) Yang, J.; Lee, J. Y.; Too, H.-P. *J. Phys. Chem. B* **2005**, *109*, 19208.

(28) Hu, J.-W.; Zhang, Y.; Li, J.-F.; Liu, Z.; Ren, B.; Sun, S.-G.; Tian, Z.-Q.; Lian, T. *Chem. Phys. Lett.* **2005**, *408*, 354.

(29) Chen, L.; Zhao, W.; Jiao, Y.; He, X.; Wang, J.; Zhang, Y. *Spectrochim. Acta, Part A* **2007**, *68A*, 484.

(30) Skrabalak, S. E.; Chen, J.; Sun, Y.; Lu, X.; Au, L.; Cobley, C. M.; Xia, Y. *Acc. Chem. Res.* **2008**, *41*, 1587.

(31) Sun, Y.; Xia, Y. *J. Am. Chem. Soc.* **2004**, *126*, 3892.

(32) Sun, Y.; Mayers, B. T.; Xia, Y. *Nano Lett.* **2002**, *2*, 481.

(33) Sun, Y.; Xia, Y. *Nano Lett.* **2003**, *3*, 1569.

(34) Sun, Y.; Wiley, B.; Li, Z.-Y.; Xia, Y. *J. Am. Chem. Soc.* **2004**, *126*, 9399.

(35) Cho, E. C.; Cobley, C. M.; Rycenga, M.; Xia, Y. *J. Mater. Chem.* **2009**, *19*, 6317.

(36) Cho, E. C.; Kim, C.; Zhou, F.; Cobley, C. M.; Song, K. H.; Chen, J.; Li, Z.-Y.; Wang, L. V.; Xia, Y. *J. Phys. Chem. B* **2009**, *113*, 9023.

(37) Ying, Y.; Chang, S. S.; Lee, C. L.; Wang, C. R. C. *J. Phys. Chem. B* **1997**, *101*, 6661.

(38) Bradley, J. S. In *Clusters and Colloids. From Theory to Applications*; VCH: Weinheim, Germany, 1994.

(39) Esumi, K.; Matsuhisa, K.; Torigoe, K. *Langmuir* **1995**, *11*, 3285.

(40) Kamat, P. V.; Flumiani, M.; Hartland, G. V. *J. Phys. Chem. B* **1998**, *102*, 3123.

(41) Sun, Y.; Xia, Y. *Science* **2002**, *298*, 2176.

(42) Liang, H.-P.; Wan, L.-J.; Bai, C.-L.; Jiang, L. *J. Phys. Chem. B* **2005**, *109*, 7795.

(43) Schwartzberg, A. M.; Olson, T. Y.; Talley, C. E.; Zhang, J. Z. *J. Phys. Chem. B* **2006**, *110*, 19935.

(44) Preciado-Flores, S.; Wang, D.; Wheeler, D. A.; Newhouse, R.; Hensel, J. K.; Schwartzberg, A.; Wang, L.; Zhu, J.; Barboza-Flores, M.; Zhang, J. Z. *J. Mater. Chem.* **2011**, *21*, 2344.

(45) Lu, X.; Tuan, H.-Y.; Chen, J.; Li, Z.-Y.; Korgel, B. A.; Xia, Y. *J. Am. Chem. Soc.* **2007**, *129*, 1733.

(46) Kim, M. H.; Lu, X.; Wiley, B.; Lee, E. P.; Xia, Y. *J. Phys. Chem. C* **2008**, *112*, 7872.

(47) Chen, J.; Saeki, F.; Wiley, B. J.; Cang, H.; Cobb, M. J.; Li, Z.-Y.; Au, L.; Zhang, H.; Kimmey, M. B.; Li, X.; Xia, Y. *Nano Lett.* **2005**, *5*, 473.

(48) Chen, J.; Wang, D.; Xi, J.; Au, L.; Siekkinen, A.; Warsen, A.; Li, Z.-Y.; Zhang, H.; Xia, Y.; Li, X. *Nano Lett.* **2007**, *7*, 1318.

(49) Wiley, B.; Sun, Y.; Chen, J.; Cang, H.; Li, Z.-Y.; Li, X.; Xia, Y. *MRS Bull.* **2005**, *30*, 356.

(50) Lu, X.; Au, L.; McLellan, J.; Li, Z.-Y.; Marquez, M.; Xia, Y. *Nano Lett.* **2007**, *7*, 1764.

(51) Prevo, B. G.; Esakoff, S. A.; Mikhailovsky, A.; Zasadzinski, J. A. *Small* **2008**, *4*, 1183.

(52) Lee, P. C.; Meisel, D. *J. Phys. Chem.* **1982**, *86*, 3391.

(53) Kim, J.-H. Ph. D. Dissertation, Department of Chemistry, University of Houston, Houston, TX, 2005.

(54) Sun, Y.; Xia, Y. *Analyst (Cambridge, U. K.)* **2003**, *128*, 686.

(55) Devarajan, S.; Bera, P.; Sampath, S. *J. Colloid Interface Sci.* **2005**, *290*, 117.

(56) Vickerman, J. C. *Surface Analysis—The Principle Techniques*; Wiley: Chichester, U.K., 1997; p 474.

(57) Reed, A. J. G.; D.C.Bell, *Energy Dispersive X-ray Analysis in the Electron Microscope (Microscopy Handbooks)*; Garland Science: New York, 2003.

(58) Rodríguez-González, B.; Burrows, A.; Watanabe, M.; Kiely, C. J.; Marzán, L. M. L. *J. Mater. Chem.* **2005**, *15*, 1755.

(59) Mie, G. *Annalen der Physik (Weinheim, Germany)* **1908**, *25*, 377.

(60) Wiley, B. J.; Chen, Y.; McLellan Joseph, M.; Xiong, Y.; Li, Z.-Y.; Ginger, D.; Xia, Y. *Nano Lett.* **2007**, *7*, 1032.

(61) Jain, P. K.; Lee, K. S.; El-Sayed, I. H.; El-Sayed, M. A. *J. Phys. Chem. B* **2006**, *110*, 7238.

(62) Sun, Y.; Tao, Z.; Chen, J.; Herricks, T.; Xia, Y. *J. Am. Chem. Soc.* **2004**, *126*, 5940.

(63) Zhang, J. Z. *J. Phys. Chem. Lett.* **2010**, *1*, 686.

(64) Goia, D. V.; Matijevic, E. *Colloids Surf., A* **1999**, *146*, 139.

(65) Wang, S.; Qian, K.; Bi, X.; Huang, W. *J. Phys. Chem. B* **2009**, *113*, 6505.

(66) Skrabalak, S. E.; Au, L.; Lu, X.; Li, X.; Xia, Y. *Nanomedicine* **2007**, *2*, 657.

(67) Skrabalak, S. E.; Chen, J.; Au, L.; Lu, X.; Li, X.; Xia, Y. *Adv. Mater.* **2007**, *19*, 3177.

(68) Au, L.; Zheng, D.; Zhou, F.; Li, Z.-Y.; Li, X.; Xia, Y. *ACS Nano* **2008**, *2*, 1645.